Cryogenic Photolysis of Activated Bleomycin to Ferric Bleomycin

Richard M. Burger,*,† Oleg M. Usov,‡ Vladimir M. Grigoryants,‡ and Charles P. Scholes*,‡

Department of Chemistry and Center for Biological Macromolecules, University at Albany, State University of New York, Albany, New York 12222, and Public Health Research Institute, 225 Warren Street, Newark, New Jersey 07103-3535

Received: July 31, 2006

Activated bleomycin (ABLM) is a drug−Fe(III)−hydroperoxide complex kinetically competent in DNA attack (via H4′ abstraction). This intermediate is relatively stable, but its spontaneous conversion to ferric bleomycin (Fe(III)·BLM) is poorly characterized because no observable intermediate product accumulates. Light was shown to trigger ABLM attack on DNA in liquid at −30 °C, so ABLM was irradiated (at its 350 nm ligand-to-metal charge-transfer transition) at 77 K to stabilize possible intermediates. ABLM photolysis (quantum yield, $\Phi = 0.005$) generates two kinds of product: Fe(III)·BLM (with no detectable intermediate) and one or more minor (1−2%) radical O−Fe−BLM byproduct, photostable at 77 K. Adding DNA, even without its target H4′, increases the quantum yield of ABLM conversion >10-fold while suppressing the observed radical yield. Since cryogenic solid-phase reactions can entail only constrained local rearrangement, the reaction(s) converting ABLM to Fe(III)·BLM must be similarly constrained.

Introduction

Activated bleomycin (ABLM: HOO^-·Fe(III)·BLM), the kinetically competent drug species, spontaneously decays to ferric bleomycin (Fe(III)·BLM) while initiating the degradation of DNA, if present,[1−3] by a 4′H abstraction.[4] The reaction pathways of ABLM formation (Scheme 1) are analogous to those of heme-containing peroxidases and oxygenases in which Fe(III) heme complexes react with HOOR or Fe(II) complexes react with O_2 and one-electron reductants.[5−7] The moderately stable ABLM ($t_{1/2} \sim 2$ min at 0 °C) provides a model for these enzymes' elusive ferric−hydroperoxy intermediate (compound 0, ref 8). But, conversely, the mechanistic details of subsequent ABLM chemistry have escaped characterization because ABLM stability presents a kinetic bottleneck that would limit the observable accumulation of any subsequent intermediate.

The reactive products of O−O scission from heme-containing peroxidases and oxygenases, known as compounds I and II,[9−12] have provided models for possible ABLM reaction intermediates. The enzymatic hydroperoxy precursor species have been cryotrapped, using reducing electrons provided by cryogenic γ irradiation, and then characterized by ENDOR (electron−nuclear double resonance) determinations of their Fe−H distances and orientation to the heme.[13,14] These enzymes can then mediate either heterolytic or homolytic O−O scission to form reactive, monooxygenated, high-valent iron intermediates and free radicals.[15,16] The organic oxidations by intermediates of P450 and other oxygenases are comparable to ABLM-mediated H-abstraction and hydroxylation at DNA-C4′, and ABLM can mediate other such enzymes' reactions as well.[17,18] ABLM O−O scission[19] is the rate-limiting step in its spontaneous (and first-order) reaction under ambient conditions in the presence or absence of DNA.[2] A DNA 4′H isotope selection effect[4,20] is consistent with an approach to an O−O scission transition state that is almost independent of 4′ H−C bond lengthening, as predicted by density functional modeling.[21] Thus O−O bond scission figures importantly in the mechanisms of both ABLM and oxygenases, although it is not yet certain in either case whether the peroxide intermediates can initiate attack directly.[15,21,22]

SCHEME 1: Activation Pathways for Iron−Bleomycins[a]

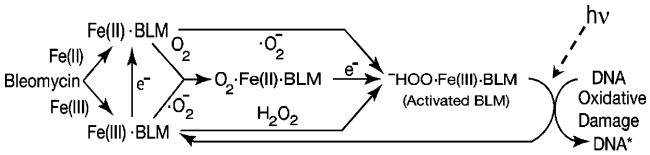

[a] The activation pathways for iron−bleomycins involve reductive activation of complexed dioxygen. The dashed arrow indicates where photolysis occurs with $h\nu$ at 350 nm, the LMCT transition.

An approach to triggering ABLM O−O scission for closer observation was suggested by the photolability of its cobalt homologue, HOO^-·Co(III)·BLM,[23−26] which is otherwise much more stable than iron ABLM, a stability that was exploited for NMR structural determinations of this ABLM model (structure **1** of Chart 1).[27−34] (The overall chemical structure of bleomycins, a ∼1.5 kD glycopeptide antitumor antibiotic family, is provided in the Supporting Information, structure **1S**.) Light triggers an attack of HOO^-·Co(III)·BLM on DNA.[23] ABLM photolysis, at its ∼350 nm (28 600 cm^{-1}) ligand-to-metal charge-transfer wavelength,[15] was conducted at 77 K to create and stabilize ABLM products, particularly for characterization by cryogenic electron paramagnetic resonance (EPR) and ENDOR spectroscopies.

Experimental Methods

Materials. Blenoxane, a gift of Bristol Laboratories, contains approximately 60% bleomycin A_2, 30% B_2, and 10% other bleomycins: it was dissolved in water and standardized opti-

* To whom correspondence should be addressed. Phone: 518-442-4551 (C.P.S.); 973-854-3155 (R.M.B.). Fax: 518-442-3462 (C.P.S.); 973-854-3101 (R.M.B.). E-mail: CPS14@albany.edu (C.P.S.); burger@phri.org (R.M.B.).

† Public Health Research Institute.

‡ University at Albany.

10.1021/jp064906o CCC: $33.50
Published on Web 09/21/2006

CHART 1: ABLM Metal Center, Showing Co(III) in Magenta (Assumed Isostructural with Fe(III)), BLM Nitrogen Ligand Macrocycle, and OOH^- with the Distal Hydroperoxy Proton Labeled H_A[a]

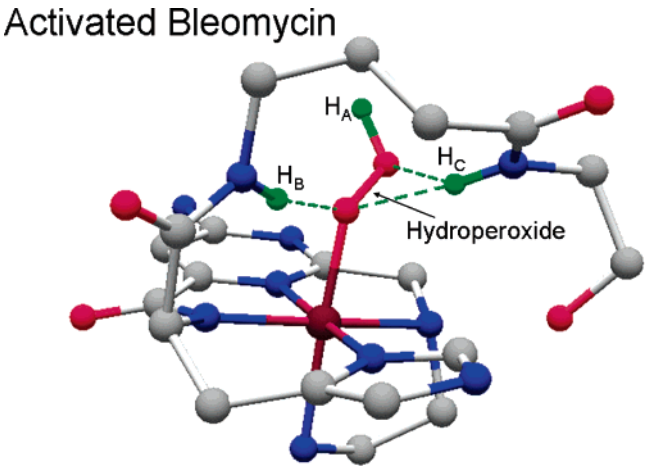

[a] The amide protons labeled H_B and H_C are sufficiently close to hydrogen bond the hydroperoxy oxygens and to provide protons for the cryophotolytic conversion of ABLM to Fe(III)·BLM. This structure is taken from the Co(III)·ABLM analogue[34] (PDB file 1MXK).

cally.[35] Calf thymus DNA was purchased from Sigma; HPLC-purified d(GGAAGCTTCC)$_2$ and d(GGAAATTTCC)$_2$ were from Oligos Etc. (Wilsonville, OR); d(GGAAG) and d(TTCC) were from TriLink (San Diego, CA). Proligo (Boulder, CO) supplied a DNA analogue lacking the bleomycin target-C_6 H4′: d(GGAAGC^{L}TTCC)$_2$, where C^L designates a 2′*O*-,4′-methylene-bridged "locked" ribocytidine. This locking modification stabilizes DNA base stacking and increases the DNA duplex dissociation temperature.[36] Temperature titrations of hyperchromicity confirmed the duplex state of all three 10-mers over 0−25 °C without annealing. Nucleic acids were dissolved in buffers, reconstituted in ^2H_2O if needed after lyophilization, and standardized optically. ^{57}Fe(II) was prepared from metallic ^{57}Fe (94 at. %, from Cambridge Isotope Laboratories (CIL, Cambridge, MA)) in dilute $^2H_2SO_4$ (Aldrich) and partially neutralized by addition of NH_4OH.[2] $^{17}O_2$ (90 at. %), ethylene glycol-$^{13}C_2$ (99 at. %), and $H_2{}^{17}O$ (84 at. %) were from Sigma-Aldrich; ^2H_2O (99.9 at. %) and perdeuterated ethylene glycol (98 at. %) was from CIL. All other chemicals were of reagent grade.

ABLM for EPR spectroscopy was prepared by adding $Fe^{II}(NH_4)_2(SO_4)_2{\cdot}6H_2O$ solution to bleomycin in sodium-phosphate buffer, pH 7.8 (unless specified) at ∼4 °C with vigorous (Vortex) mixing under air (for Fe < 0.4 mM) or O_2 (for Fe ≥ 0.4 mM). This method of preparing ABLM in phosphate buffer creates a 1:1 mixture of low spin ferric ABLM and high spin ferric Fe(III)·BLM (g = 4.3), the latter readily distinguished from the low spin ferric Fe(III)·BLM and ABLM by EPR. The high spin state of Fe(III)·BLM in phosphate buffer may reflect phosphate becoming an iron ligand and weakening the iron ligand field. DNA, if desired, was added next and then ethylene glycol (to 50% (v/v)), and the mixture was transferred to a quartz EPR tube and frozen in liquid N_2 within ∼1 min of Fe(II) addition. At 4 °C, in phosphate buffer, ABLM converts to Fe(III)·BLM with $t_{1/2}$ ∼ 2 min.[2] In samples with phosphate buffer (but no DNA) the low spin Fe(III)·BLM product of ABLM cryophotolysis is readily distinguished from high spin Fe(III)·BLM produced spontaneously before freezing.[1,2,37] For samples prepared in protonated solvent, in deuterated solvent, in deuterated solvent with ^{57}Fe, and in deuterated solvent with dioxygen-^{17}O, the ^{57}Fe and ^{17}O showed their previously documented spectral effects on ABLM prior to photolysis and on the low spin Fe(III)·BLM EPR spectra.[2] As was done previously, samples of entirely low spin ferric Fe(III)·BLM were prepared from $Fe^{III}(NH_4)(SO_4)_2{\cdot}12H_2O$ plus BLM in 20 mM Na−HEPES, pH 7.8.[38−40]

Spectroscopic Methods. X-band EPR (9.52 GHz) was measured with an ER-200 IBM Bruker X-band spectrometer equipped with a standard TE_{102} EPR cavity and an LTR-3 Helitran system (APD Cryogenics, Allentown, PA) that controlled temperature in the 6−50 K range. X-band spectroscopy was performed on samples in 3 mm (Wilmad, Buena, NJ) or 2 mm i.d. (Vitrodynamics, Mountain Lakes, NJ) quartz tubes at 15 K unless otherwise noted, and data were collected in a PC using the EW Software routines (Scientific Software Services, Plymouth, MI). Q-band (34.1 GHz) ENDOR measurements were performed on 2 mm i.d. samples under dispersion (χ'), rapid passage field-modulated conditions with a cryogenically tunable TE_{011} Q-band resonator[41] as previously reported,[42−44] at 2 K, using a data accumulation software package previously described. Optical absorbance was measured with a Shimadzu model UV-1601 spectrophotometer.

For quantitation of Fe(III)-BLM species by EPR, the proportionality of their EPR derivative features to their concentrations was first determined by interconverting these species in a single sample as previously described.[2] ABLM was estimated by derivative peak height at g_3 = 1.94, low spin Fe(III)·BLM) by derivative peak height at g_3 = 1.89, and high spin Fe(III)·BLM by peak-to-peak derivative height at g = 4.3. (The same g = 1.89 line shape is seen with Fe(III)·BLM formed either by de novo complexation in HEPES, by ABLM decay at 4 °C, or by photolysis at 77 K.) The novel radical species were quantitated by their doubly integrated EPR derivatives and comparison to those of ABLM and Fe(III)·BLM. The course of photolysis was estimated by fitting species concentration versus irradiation as described immediately below.

Sample Irradiation. EPR tubes were irradiated at 350 nm, when desired, under liquid N_2 in a narrow, quartz insert X-band EPR sample dewar (Wilmad), within a Rayonet Photochemical Reactor ("Srinivason-Griffin" model, Southern New England Ultraviolet Co., Hamden, CT). The incident light intensity was determined by ferrioxylate actinometry,[45] using briefly irradiated actinometry samples (of acid $K_3Fe(C_2O_4)_3$) matched in geometry and A_{350} to the photolyzed samples. Photoreduction to Fe(II) was then assayed by A_{510} after complexation with added 1,10-phenanthroline.[45] (Incident light intensity and absorbance are given in einsteins/min, where one einstein = 1 mol of photons). In 3 mm EPR tubes 0.2 mL samples received 1.66 μeinsteins/min; in 2 mm tubes 0.06 mL samples received 0.56 μeinstein/min. At 350 nm ABLM and Fe(III)·BLM have almost identical absorbencies (∼3000 M^{-1} cm^{-1})[2,46] and are the only light-absorbing species in the samples. The absorption in all samples approached 100%. The amounts of ABLM and Fe(III)·BLM in each sample were estimated by EPR spectrometry before and after partial photolysis, and quantum yields of ABLM photolysis (Φ = ΔABLM per equiv light it absorbed) were obtained from the initial rates of ABLM cryophotolysis, calculated from the rate constant of the single-exponential decay that fit the course of photolysis. The possibility was addressed that the finite thickness of the sample and absorbances of ABLM and Fe(III)·BLM might significantly diminish the flux in the interior of our 2 or 3 mm sample tubes and thereby distort the photolysis kinetics, but calculations showed that this would be negligible in our samples (A_{350} ≈ 3 cm^{-1}).

Reactions of ABLM with DNA. Incubations for cleavage of DNA or oligonucleotide, to assay ABLM activity, were conducted at 0 °C unless otherwise stated, in polypropylene tubes. ABLM was formed by adding Fe(II) solution to aerobic, phosphate-buffered BLM. Cleavage was assayed colorimetrically[46] by means of the stoichiometric product,[47] base propenal (trivial name for 3-(pyrimidin-1′-yl)-2-propenals and 3-(purin-9′-yl)-2-propenals[48]), which forms a chromophore with 2-thiobarbituric acid (product $\epsilon_{532} = 1.58 \times 10^5\ mM^{-1}$).[49] DNA cleavage reactions were terminated by adding ≥3 vols of TBA reagent (42 mM 2-thiobarbituric acid, 1 mM EDTA),[46] and, after 20 min at 90 °C and then cooling, A_{532} was measured. Additionally, the oxygen-independent formation of 4′-keto abasic lesions by ABLM makes DNA alkali-labile.[4,50] These lesions were assayed using HPLC analysis of intact and cleaved 10-mers, d(G-GAAGCTTCC)$_2$ before and after treatment at pH 11.5 for 10 min at 65 °C followed by neutralization. A reversed phase C-18 column (15 × 0.4 cm, 5 μm beads), was eluted at 1 mL/min with 0−30% acetonitrile, 0.1 M triethylammonium acetate, pH 6.5 over 15 min.

Colder, liquid-phase DNA cleavage reactions (−30 °C, Table 1) were conducted within a 10 cm clear quartz dewar containing a 44% ethylene glycol bath chilled by submerged dry ice chips. The thermocouple-monitored temperature was maintained within 0.5 °C. Corex incubation tubes of 15 mL each were suspended in the dewar (within the Rayonet Photochemical Reactor), and each contained 0.1 mL in which ∼75 μM ABLM absorbed ∼20 μeinsteins over 1 h. Some tubes were masked with foil for unirradiated controls. Reactions were initiated by adding 2 μL of $Fe^{II}(NH_4)_2(SO_4)_2$ solution to the other chilled constituents (98 μL, 45% ethylene glycol). For termination, TBA was added, followed by assay of base propenal. Actinometry was performed as above using matched samples.

Proton ENDOR Interpretation. The frequencies of proton ENDOR features, $^{P}\nu_{ENDOR}$, center, to first order, at the free proton nuclear Zeeman frequency, ν_P. Taking A as the hyperfine coupling, one finds the ENDOR frequencies to be split away from ν_P by $\pm^1/_2A$ for protons coupled to the electron spin $^1/_2$ doublet. Thus, proton ENDOR frequencies, occurring as "+" or as "−" Zeeman branches, are[51]

$$^{P}\nu^{\pm}_{ENDOR} = |\nu_P \pm A/2| \quad (1)$$

First-order expressions for ENDOR frequencies hold when $\nu_P \gg A/2$, as is the case here with a magnetic field of ∼1.2 T and ν_P in the 50 MHz range. For the work reported here, where hyperfine couplings are measured at a particular g-value, often at the maximal g-value g_1 for a particular low spin ferric species, the hyperfine coupling is given the designation $A(g_1)$.[7] Under rapid passage conditions the intensity of the "+" and the "−" branches need not be the same.[39,43,51,52] However, the major information from ENDOR is in the frequency of features from which hyperfine couplings are derived and not in the ENDOR intensity, which may be affected by spin relaxation, RF, and microwave power levels. ν_P and the measured $^{P}\nu_{ENDOR}$ of the "−" branch suffice to determine A.

Results

Liquid-Phase ABLM Photolysis. In −30 °C solutions in the dark, DNA cleavage by ABLM is slow. Measured by production of its stoichiometric product, base propenal, it was only 14% complete in 1 h, as compared to an incubation mixture subsequently warmed for completion at 25 °C (Table 1).

TABLE 1: Effect of Light on DNA Cleavage (Base Propenal) Yield in Liquid

incubation with ABLM[a]:	base propenal yield (μM)	
	1 h at −30 °C	plus 5 min at 25 °C (dark)
in dark	3.9	28.2
in light (350 nm)	13.3	27.1

[a] Samples (0.1 mL) contained 0.22 mM bleomycin, 1.3 mM calf thymus DNA (nucleotides), 20 mM sodium-phosphate buffer, pH 7.8, and 44% (v/v) ethylene glycol; 0.20 mM $Fe^{II}(NH_4)_2(SO_4)_2 \cdot 6H_2O$ was added last to initiate reactions at −30 °C. The irradiated samples received 52 μeinsteins over 1 h. For reaction termination and base propenal assay, 0.7 mL TBA was added.

A −30 °C incubation mixture illuminated 1 h at 350 nm achieved 49% completion, over triple the rate in the dark at that temperature. Thus, light triggers DNA cleavage by ABLM under cold liquid conditions. When the partially photolyzed sample is warmed to room temperature, it provides the same final cleavage yield as shown by a control sample kept dark—and very similar to another incubation conducted entirely at room temperature. Thus, the DNA product of photolysis in cold liquid is identical to that of spontaneous, dark, ABLM action, and the photolysis does not alter the stoichiometric cleaving efficiency. The −30 °C DNA cleavage due to photolysis (Table 1) shows a quantum yield $\Phi \approx 5 \times 10^{-4}$ (9.4 nmol additional base propenal per 20 μeinsteins absorbed by ABLM). Since cleavage (under atmospheric O_2) is usually accompanied by approximately equal formation of its alternative 4′-keto abasic lesion,[53] the overall ABLM quantum yield is probably $\sim 10^{-3}$.

ABLM Photolysis at 77 K. The spontaneous cleavage of DNA by ABLM is even slower at lower temperatures. Cryophotolysis (in a glass) leads neither to DNA cleavage nor to 4′-keto abasic lesions (data not shown). Instead, ABLM and its cryophotolysis products were monitored by EPR spectroscopy at 15 K after illumination at 77 K in a 50% ethylene glycol glass kept at ≤77 K. Over 0−80 min of irradiation (0−133 μeinsteins/sample), the spectrum of ABLM (g_1, g_2, g_3 = 2.26, 2.17, 1.94) was supplanted by that of its usual product, Fe(III)·BLM (g_1, g_2, $g_3 \approx$ 2.42, 2.18, 1.89) as shown in Figure 1 with a sample prepared at natural isotopic abundance. Under ambient conditions in the phosphate buffer used, Fe(III)·BLM is high spin ferric but, when produced by cryophotolysis of ABLM, it is low spin until thawed. Figure 1S (Supporting Information) compares the low spin X-band spectra of ABLM to those of its Fe(III)·BLM products after 20 min (partial) cryophotolysis for samples respectively prepared in natural protonated solvent, in deuterated solvent, and in deuterated solvent with ^{57}Fe or dioxygen-^{17}O. Figure 2S (Supporting Information) shows the only EPR difference between Fe(III)·BLM produced by cryophotolysis and by mixing Fe(III) with BLM: a 0.02 decrease in the value of g_1.

Origin of the H_2O Ligand of Fe(III)·BLM Produced Cryophotolytically. Following the cryophotolysis of ^{17}O-ABLM, which itself displays a broadened g_2 (intermediate g-value feature) (Figure 1S), a previously unseen[2] broadening of the Fe(III)·BLM g_2 feature is conspicuous. The comparison of g_2 EPR line widths of ^{16}O- and the ^{17}O-Fe(III)·BLM samples (30 vs 50 G) made by complete cryophotolysis of ABLM is provided in the top two traces of Figure 2. The implication of the broadening is that, following hydroperoxide cryophotolysis, a ^{17}O atom remains in situ as the H_2O oxygen ligand of Fe(III)·BLM. The ^{17}O-broadened species can also be made using $H_2{}^{17}O$ when mixing solutions of Fe(III) and BLM, as shown by the bottom spectrum of Figure 2.

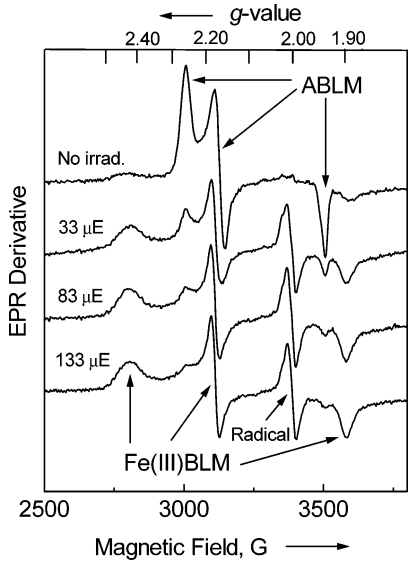

Figure 1. X-band EPR spectra of ABLM cryophotolyzates. The sample (0.2 mL, natural isotopic abundance) received 1.65 μeinsteins/min at 350 nm for 0, 20, 50, and 80 min at 77 K; it contained 1 mM Fe, 1.1 mM BLM, 20 mM sodium-phosphate buffer, pH 7.8, and 50% (v/v) ethylene glycol. High spin Fe(III)·BLM ($g = 4.3$, not shown) constitutes about half the Fe−BLM in this sample. These spectra were obtained at 15 K, 6 G field modulation, 200 s of spectrum accumulation, 2 mW power, and $\nu_{EPR} = 9.525$ GHz. Note that the cryophotolytically produced Fe(III)·BLM remains low spin even though Fe(III)·BLM prepared de novo in phosphate buffer would be high spin.

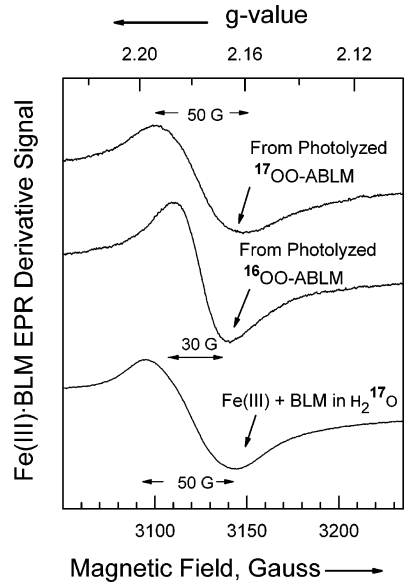

Figure 2. Effects of oxygen isotopes on Fe(III)·BLM EPR line width. Compare the broadened Fe(III)·BLM (at g_2) from cryophotolyzed ^{17}OO-ABLM (0.5 mM in 20 mM sodium-phosphate buffer, pH 7.8) to that of Fe(III)·BLM from ^{16}OO-ABLM in an otherwise identical sample. Fe(III)·BLM from cryophotolyzed ^{17}OO-ABLM and Fe(III)·BLM dissolved in water-^{17}O (HEPES buffer) have identical EPR line broadening. Spectroscopic conditions were as for Figure 1.

Similar Local Structure of Fe(III)·BLM Prepared Directly and by Cryophotolysis of ABLM Revealed by ENDOR of Exchangeable Protons. The underlying proton features of Fe(III)·BLM are sensitive to the coordinating BLM ligand structure and the axial Fe ligand.[54] These proton couplings are largest at $g_1 = g_{max}$, are consistent with the expected dipolar coupling to axial water, and are different from those observed from ABLM. The ENDOR spectra here simply present an experimental probe of local structure, and angle-selected ENDOR versus g-value

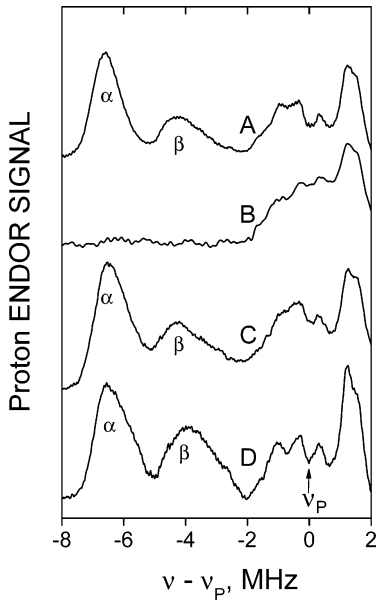

Figure 3. Exchangeable, strongly coupled, proton ENDOR of Fe(III)·BLM. Spectra are from (A) Fe(III)·BLM (2 mM) prepared de novo under ambient conditions from Fe(III) and BLM, no DNA, (HEPES buffer); (B) as in (A) but in deuterated solvent; (C) Fe(III)·BLM from cryophotolysis of ABLM (0.5 mM) with no DNA present (phosphate buffer); (D) Fe(III)·BLM from cryophotolysis of ABLM (0.6 mM) in the presence of 0.7 mM d(GGAAGCTTCC)$_2$ (HEPES buffer). The conditions for proton ENDOR spectra were $H = 10075$ G ($\nu_P = 42.89$ MHz, $g_1 = 2.418$) for Fe(III)·BLM. Spectra were obtained under adiabatic rapid passage conditions at 2.0 K with large (~2.2 G) 100 kHz field modulation, ~0.25 μW microwave power, and ~20 W RF (radio frequency) pulsed with a 10 μs/90 μs duty cycle and swept at 4 MHz/s. Each spectrum was compiled in ~10 min.

will be presented elsewhere to provide the details of angles and distances to these nearby exchangeable protons.

The strongly coupled exchangeable proton ENDOR observed at g_1 are compared in Figure 3. As was found for rapid passage ENDOR of the peroxidases and oxygenases at their g_1 extremum,[5,7,55] the $^{P}\nu^{-}_{ENDOR}$ branch, located below the free proton NMR frequency, is more intense than the $^{P}\nu^{+}_{ENDOR}$ branch. The couplings, $A(g_1)$, can be readily estimated from the $^{P}\nu^{-}_{ENDOR}$ branch, shown here. Spectrum 3B, of Fe(III)·BLM in deuterated solvent, shows that the exchangeable protons are responsible for the labeled outlying features. The spectra of directly complexed Fe(III) + BLM in HEPES buffer (spectrum 3A), of Fe(III)·BLM formed by cryophotolysis of ABLM in the absence of DNA (Figure 3C) in phosphate buffer, and of Fe(III)·BLM formed by cryophotolysis at 77 K with d(GGAAGCTTCC)$_2$ present (spectrum 3D) differed but slightly. The features α and β respectively had couplings $A(g_1) = 13.2$ and 7.8−8.5 MHz.

Radical EPR Spectra. Together with the conversion of ABLM to Fe(III)·BLM, a complex radical spectrum appears near $g = 2.00$ having features sensitive to exchangeable protons, ^{57}Fe, and ^{17}O of the initial ABLM (Figure 4). The radicals did not form in irradiated controls lacking ABLM, even those containing Fe(III)·BLM. This spectral product was refractory to further 350 nm illumination or storage at 77 K but disappeared on thawing. Except for exchangeable H, no solvent nucleus (i.e., ^{17}O of $H_2{}^{17}O$ or the covalently attached ^{1}H or ^{13}C of ethylene glycol) affected the cryophotolytically produced radical EPR spectra. The comparison of radicals induced by ABLM cryophotolysis in natural or perdeuterated solvent distinguished between exchangeable and nonexchangeable H hyperfine features. The finer spectral resolution of the radical in perdeuterated solvent also clarified hyperfine changes attributable to both

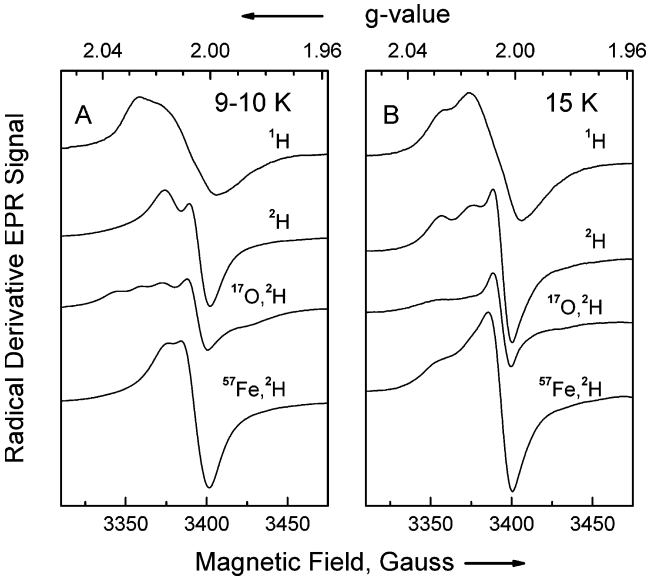

Figure 4. Effects of ^{1}H, ^{2}H, ^{17}O, and ^{57}Fe spin isotopes on EPR spectra of radicals from cryophotolyzed ABLM. Samples of ABLM (0.5 mM in 20 mM sodium-phosphate buffer, pH 7.8) were prepared with either natural abundance constituents (^{1}H), perdeuterated solvents (^{2}H), $^{17}O_2$ and ^{2}H, or ^{57}Fe and ^{2}H, as shown. Irradiation was 320 einsteins/mol of ABLM. The spectra of A were obtained at 9−10 K and of B at 15 K. EPR conditions were 3 G field modulation, 200 s total signal accumulation over the field range shown, 2 mW power, and ν_{EPR} = 9.525 GHz.

^{57}Fe ($I = {}^1/_2$) and $^{17}O_2$ ($I = {}^5/_2$) products, and the ^{17}O-derived features are particularly conspicuous in Figure 4A. Figure 4 additionally shows radical sensitivity to changing the temperature between 9 and 15 K. The effects of temperature on the radical spectra from ABLM photolyzed in perdeuterated solvent (Figure 3S, Supporting Information) include major changes over 6−50 K, and these changes are reversible with temperature. The radicals must reside near the Fe and O from ABLM. Although the bleomycin iron ligands include five nitrogens (Chart 1), we have detected no obvious nitrogen participation in the radical. These radicals were not further characterized with regard to structure or additional nuclei involved. Despite their conspicuous EPR derivative spectra, the radicals shown constitute only 1−2% of the original Fe−BLM spins, so ENDOR characterization of them was prevented by the superimposed signals of Fe(III)·BLM and ABLM.

Effect of DNA on the Course of ABLM Cryophotolysis. The progressive conversion of ABLM (without DNA present) to Fe(III)·BLM and radical EPR species is shown in Figure 5. These three species were monitored over time and photon dose using EPR spectrometry as described under Experimental Methods. Since the radicals appear almost simultaneously with the conversion of ABLM to Fe(III)·BLM and persist after ABLM photolysis is complete (Figure 1), they and Fe(III)·BLM are alternative products of cryogenic ABLM photolysis. As quantitated, the photolytically produced Fe(III)·BLM accounted for approximately two-thirds of the decrease in the ABLM; thus it is possible that some products of ABLM photolysis, unlike Fe(III)·BLM, escape EPR detection.

When DNA is present during ABLM irradiation, the cryophotolysis quantum yield increases over an order of magnitude. The progress of ABLM cryophotolysis is shown in the presence and absence of calf thymus DNA (Figure 6). The effect of DNA on the photolysis quantum yield far exceeds its minor effect (<1.3-fold) on the rate of spontaneous ABLM decay in phosphate buffered solutions.[2] This is consistent with DNA

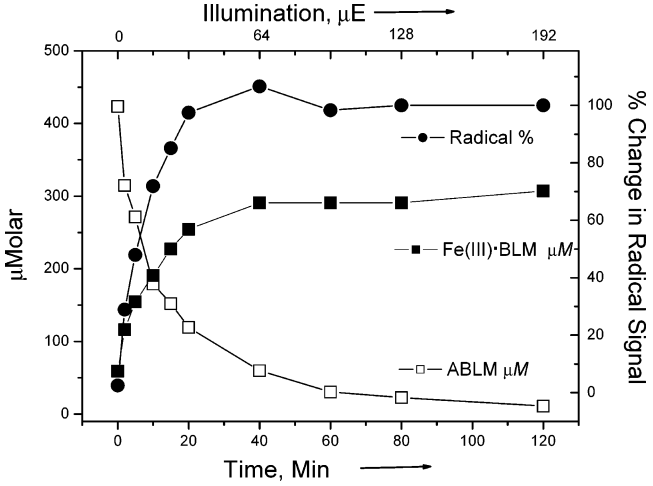

Figure 5. Reaction course of ABLM cryo-photolysis: comparison of signal amplitudes from ABLM, Fe(III)·BLM, and the radical peak. The sample contained ABLM prepared without DNA in protonated solvent. [ABLM] was estimated by the EPR $g = 1.94$ derivative, [Fe(III)·BLM] was estimated by the EPR $g = 1.89$ derivative, and the radical intensity was estimated from the peak-to-peak derivative height of the radical, all as measured for Figure 1.

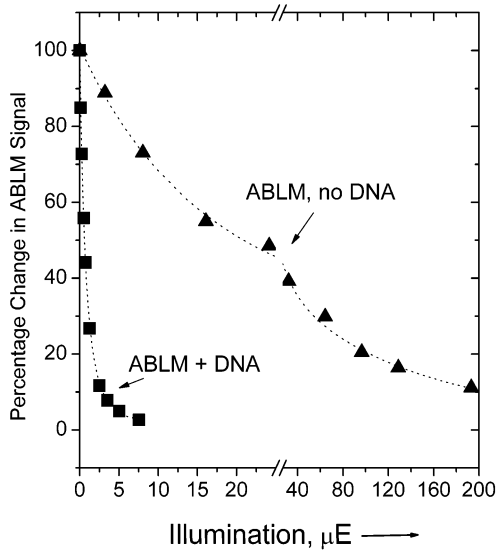

Figure 6. Change in ABLM cryophotolysis upon DNA addition. The percentage change in ABLM was estimated by the $g = 1.94$ EPR signal, measured as for Figure 1. The quantum yield (efficiency) of photolysis is markedly increased by the presence of DNA; these 0.2 mL samples contained 1 mM Fe−BLM with 5 mM DNA.

TABLE 2: Quantum Efficiency (Φ) of ABLM Cryophotolysis

DNA present	Φ[a]
none	0.0053 ± 0.0005
calf thymus DNA	0.063 ± 0.008
d(GGAAGCTTCC)$_2$	0.065 ± 0.015
d(GGAAATTTCC)$_2$	0.087 ± 0.012
d(GGAAGC^{L}TTCC)$_2$	0.085 ± 0.012

[a] Errors calculated from the computed initial rate of cryophotolysis.

changing the interaction of ABLM and light without the DNA otherwise labilizing the O−O bond. The >10-fold increase in quantum yield occurred both with heterogeneous (calf thymus) DNA and several oligonucleotide duplexes that differ in their susceptibility to ABLM under ambient conditions,[56] as shown in Table 2. These oligonucleotides were (1) d(GGAAGCTTCC)$_2$, which contains a single preferred d(GpC) target sequence

that specifically binds to the bleomycin and is targeted for attack by ABLM;[57,58] (2) the analogous d(GGAAATTTCC)$_2$, which contains no d(GpC) or d(GpT) target sequence and that binds less specifically to bleomycin;[56] (3) the uncleavable (<1%: Table 1S of the Supporting Information) analogue d(GGAAGC^L-TTCC)$_2$, where C^L designates the 2′O-,4′-methylene-bridged target rC$_6$. (For the course of ABLM photolysis with d(G-GAAGC^{L}TTCC)$_2$ present see Supporting Information, Figure 4S.) In case 3 the large increase in cryophotolysis quantum yield occurs even though the DNA target H4′ [4] is absent. This uncleavable oligonucleotide did not inhibit cleavage of its natural analogue (Table 1S in the Supporting Information) under ambient conditions, but its effect at enhancing the cryogenic photolysis of ABLM indicates that it still interacts with ABLM.

Discussion

The activity of photolysis-triggered DNA cleavage by ABLM (in −30 °C liquid) is analogous to that of spontaneously reacting ABLM. Both are detected by formation of base-propenal, a stoichiometric DNA cleavage product.[47] The final DNA cleavage yield of photolyzed ABLM (at −30 °C) is the same as that of spontaneously reacting ABLM. The Fe(III)·BLM product of ABLM cryophotolysis in a 77 K glass has the same EPR and ENDOR signatures as the product formed spontaneously (in HEPES) at ambient temperature. A broadened EPR line width at g_2 was a definitive reporter for ^{17}O in ABLM.[2] Now the g_2 region of Fe(III)·BLM, whether produced cryophotolytically from ^{17}OO-ABLM or prepared by addition in liquid $H_2{}^{17}O$, shows, by an identical broadening, that the photolysis process yields bound $H_2{}^{17}O$ (or $^{17}OH^-$) from the cleaved hydroperoxide-^{17}O. The exchangeable proton ENDOR, which would include that of the bound H_2O, is identical for Fe(III)·BLM made at ambient temperature (in HEPES) and for Fe(III)·BLM generated from ABLM. Two differences seen between the liquid phase and the cryophotolytic reactions are that, with the latter, (a) DNA, when present, does not suffer its usual lesions and (b) unusual radical species arise that show EPR evidence of nearby ^{17}O and ^{57}Fe tracers. The importance of cryogenic photolysis of ABLM in understanding the basis of ABLM reactivity is as follows:

Electronic Structural Basis of ABLM Photolysis. The optical transition at the wavelength used to drive photolysis is that of the 350 nm ligand-to-metal charge transfer (LMCT),[15] thought to arise from a shift of electron density to the metal from orbitals at the deprotonated amide of the bleomycin. The calculations of Neese, Solomon, and co-workers[15,16,21] indicate that at ambient temperature with DNA present the breaking of the relatively weak hydroperoxide O−O bond is coupled to the abstraction of DNA-H4′. Because neither cryophotolytic nor ambient, spontaneous, hydroperoxide scission require DNA to be present, an accessible H4′ is not necessary for these reactions. The 350 nm photon, having an energy of 82 kcal/mol, can provide an activation energy not thermally available even at ambient temperatures. Thus, it is possible that an optically driven LMCT might induce a metal charge transfer to an antibonding orbital of the hydroperoxide ligand, leading to O−O bond scission. The likelihood of electron transfer to the hydroperoxide will depend on the orientation of the hydroperoxide ligand with respect to metal d orbitals, and the orientation of the hydroperoxide might be modulated by the presence or absence of DNA,[32] thus providing a rationale for the enhanced quantum yield of ABLM photolysis in the presence of DNA. However, since DNA has little if any effect on spontaneous ABLM O−O scission (<1.3-fold), it seems more likely that the effect of DNA at 77 K (>10-fold) is not exerted directly on the O−O bond stability or that the hydroperoxide orientation is less important for its scission at ambient temperature. The LMCT excited state resulting from an electron transferred from bleomycin to metal could produce a radical, localized on the bleomycin macrocycle, which might, if stable at 77 K, account for the minority radical species observed. The density functional treatment of ABLM was addressed to the energetic cost of heterolytic, homolytic, and H-abstraction mechanisms for hydroperoxide scission.[21] It would be desirable to enlist such a treatment to explain the detailed photolytic mechanism of ABLM O−O hydroperoxide bond scission and its perturbation by DNA as well as the possibility of forming unusual radicals. The absence of any detected intermediate in the conversion of ABLM to Fe(III)·BLM is consistent with a direct reaction but not a proof. Continuing investigations of this process at lower temperatures and shorter time intervals could strengthen or disprove the assertion that there is no intermediate.

Fe(III)·BLM Product of Photolysis. The EPR spectra of Fe(III)·BLM, whether as prepared de novo or by cryophotolysis of ABLM, are virtually identical. However, the maximal *g*-value (≈2.42, Supporting Information, Figure 2S) was slightly less in the cryophotolytically produced Fe(III)·BLM, so the splitting of its metal t_{2g} orbitals may differ slightly from that of the Fe(III) + BLM mixture.

The comparison of Fe(III)·BLM prepared cryophotolytically from ^{17}OO- or ^{16}OO-ABLM shows unambiguously that the H_2O ligand of Fe(III)·BLM derives from the dioxygen of ABLM. The strongly coupled exchangeable protons of Fe(III)·BLM observed by ENDOR, which would include those of its H_2O ligand, must originate near the ligated Fe(III) in ABLM. The NMR study of the Co(III) homologue of ABLM shows that the peptide chain[27−34] contains two amide protons directed toward the proximal oxygen, which are labeled H_A and H_C in structure **1**. One or both of these could become a H_2O proton of the Fe(III)·BLM cryophotolytic product.

Unless ABLM photolysis releases a 2e$^-$ oxidant species, conversion of ABLM to a ferri−aquo BLM complex requires a 2e$^-$ reduction, which may be performed internally by some BLM moiety. When the residual activity of photolyzed ABLM was assayed after addition of DNA and more Fe(II), it was found to be diminished, like that of "redox inactivated" ABLM, which had been permitted to decay spontaneously. In neither cryophotolyzed ABLM nor redox inactivated ABLM has any unique damage been unambiguously characterized. Preliminary efforts to characterize such damage by MS, NMR, or optical changes in the BLM moiety are in progress.

Radical Species Produced. Although it is common to find radicals produced during photolysis, the ones described here depend on ABLM for formation, and they report nearby nuclei present in the initial ABLM. It is not clear if the radical species are byproducts of the prevalent pathway to Fe(III)·BLM or of a different reaction mode. Several potential modes of ABLM hydroperoxide scission have been proposed involving heterolytic or homolytic scission or this latter with hydrogen abstraction.[11] Heterolytic scission requires considerable activation,[15] but the 82 kcal/mol photon could in principle provide this. The unusual nature of the radical is evident in the hyperfine contributions of ^{17}O and ^{57}Fe (derived from ABLM) and the radicals' temperature dependence, a feature of radicals spin-coupled to Fe, such as those found in high valent iron−oxo porphyrin analogues of compound I.[59] Although the stoichiometric propor-

tion of the radical product species was small, their very existence suggests that cryophotolysis can provide a high valent iron−oxo species that had been thought too energetic to occur as ambient temperature intermediates.

Conclusions

The demonstrated cryophotolytic conversion of ABLM to Fe(III)·BLM may proceed by providing access to the excited electronic states of ABLM that permit O−O peroxide bond scission. Cryogenic ABLM photolysis experiments show that (1) spectroscopically identified low spin Fe(III)·BLM is formed with no detectable intermediate, at 77 K, upon ABLM photolysis with DNA either absent or present; (2) the presence of DNA conveys a >10-fold enhancement in the quantum yield of ABLM cryophotolysis; and (3) minor quantities of conspicuous radicals also form, having an unusual complexity and reversible temperature dependence in the region of 6−50 K. They are photostable at 77 K and show proximity of exchangeable protons, ^{57}Fe, and ^{17}O, whenever these were initial ABLM constituents—thus indicating an iron-oxy character.

Acknowledgment. These studies were partially supported by NIH (Grant EB00326929, C.P.S.). We are grateful to Dr. Berry Birdsall, NIMR Mill Hill, U.K., for NMR spectroscopy, to Drs. Fred Kramer, Sanjay Tyagi, and Salvatore A. E. Marras, Public Health Research Institute, Newark, NJ, for HPLC analyses of oligonucleotide degradation products, and to Dr. Harvey Penefsky, Public Health Research Institute, Newark, NJ, for a preliminary 0 °C photolysis trial.

Supporting Information Available: Structure **1S**, showing the complete structure of bleomycin, Figure 1S, showing the effects of ^{1}H, ^{2}H, ^{17}O, and ^{57}Fe spin isotopes on EPR spectra of ABLM cryophotoproducts, Figure 2S, comparing the X-band EPR spectrum of the g_1 region from Fe(III)·BLM following cryophotolysis of ABLM and Fe(III)·BLM as prepared de novo by addition of Fe(III) to BLM, Figure 3S, showing the temperature-dependent interconversions of the photolyzed ABLM radical in the 6−50 K range, Figure 4S, showing cryophotolysis with d(GGAAGC^{L}TTCC)$_2$ present, and Table 1S, comparing the effect of a 2′*O*-,4′-methylenylcytidine (C^{L}) on DNA cleavage. This material is available free of charge via the Internet at http://pubs.acs.org.

References and Notes

(1) Kuramochi, H.; Takahashi, K.; Takita, T.; Umezawa, H. *J. Antibiot.* **1981**, *34*, 578.
(2) Burger, R. M.; Peisach, J.; Horwitz, S. B. *J. Biol. Chem.* **1981**, *256*, 11636.
(3) Burger, R. M. *Chem. Rev.* **1998**, *98*, 1153.
(4) Wu, J. C.; Kozarich, J. W.; Stubbe, J. A. *Biochemistry* **1985**, *24*, 7562.
(5) Davydov, R.; Macdonald, I. D. G.; Makris, T. M.; Sligar, S. G.; Hoffman, B. M. *J. Am. Chem. Soc.* **1999**, *121*, 10654.
(6) Schlichting, I.; Berendzen, J.; Chu, K.; Stock, A. M.; Maves, S. A.; Benson, D. E.; Sweet, R. M.; Ringe, D.; Petsko, G. A.; Sligar, S. G. *Science* **2000**, *287*, 1615.
(7) Davydov, R.; Makris, T. M.; Kofman, V.; Werst, D. E.; Sligar, S. G.; Hoffman, B. M. *J. Am. Chem. Soc.* **2001**, *123*, 1403.
(8) Kettle, A. J.; Winterbourne, C. C. *J. Biol. Chem.* **1992**, *267*, 8319.
(9) Theorell, H.; Ehrenberg, A.; Chance, B. *Arch. Biochem. Biophys.* **1952**, *37*, 237.
(10) Thomas, J. A.; Morris, D. R.; Hager, L. P. *J. Biol. Chem.* **1970**, *245*, 3135.
(11) Dawson, J. W. *Science* **1988**, *240*, 433.
(12) Sono, M.; Roach, M. P.; Coulter, E. D.; Dawson, J. H. *Chem. Rev.* **1996**, *96*, 2841.
(13) Davydov, R.; Chemerisov, S.; Werst, D. E.; Rajh, T.; Matsui, T.; Ikeda-Saito, M.; Hoffman, B. M. *J. Am. Chem. Soc.* **2004**, *126*, 15960.
(14) Davydov, R.; Kofman, V.; Fujii, H.; Yoshida, T.; Ikeda-Saito, M.; Hoffman, B. M. *J. Am. Chem. Soc.* **2002**, *124*, 1798.
(15) Neese, F.; Zaleski, J. M.; Zaleski, K. L.; Solomon, E. I. *J. Am. Chem. Soc.* **2000**, *122*, 11703.
(16) Lehnert, N.; Neese, F.; Ho, R. Y. N.; Que, L.; Solomon, E. I. *J. Am. Chem. Soc.* **2002**, *124*, 10810.
(17) Padbury, G.; Sligar, S. G. *J. Biol. Chem.* **1985**, *260*, 7820.
(18) Murugesan, N.; Hecht, S. M. *J. Am. Chem. Soc.* **1985**, *107*, 493.
(19) Burger, R. M.; Tian, G.; Drlica, K. *J. Am. Chem. Soc.* **1995**, *117*, 1167.
(20) Kozarich, J. W.; L. Worth, J.; Frank, B. L.; Christner, D. F.; Vanderwall, D. E.; Stubbe, J. *Science* **1989**, *245*, 1396.
(21) Decker, A.; Chow, M. S.; Kemsley, J. M.; Lehnert, N.; Solomon, E. I. *J. Am. Chem. Soc.* **2006**, *128*, 4719.
(22) Ogliaro, F.; de Visser, S. P.; Cohen, S.; Sharma, P. K.; Shaik, S. *J. Am. Chem. Soc.* **2002**, *124*, 2806.
(23) Chang, C. H.; Meares, C. F. *Biochemistry* **1982**, *21*, 6332.
(24) Chang, C. H.; Meares, C. F. *Biochemistry* **1984**, *23*, 2268.
(25) Subramanian, R.; Meares, C. F. *J. Am. Chem. Soc.* **1986**, *108*, 6427.
(26) Saito, I.; Morii, T.; Sugiyama, H.; Matsuura, T.; Meares, C. F.; Hecht, S. M. *J. Am. Chem. Soc.* **1989**, *111*, 2307.
(27) Wu, W.; Vanderwall, D. E.; Stubbe, J.; Kozarich, J. W.; Turner, C. J. *J. Am. Chem. Soc.* **1994**, *116*, 10843.
(28) Wu, W.; Vanderwall, D. E.; Lui, S. M.; Tang, X.-J.; Turner, C. J.; Kozarich, J. W.; Stubbe, J. *J. Am. Chem. Soc.* **1996**, *118*, 1268.
(29) Wu, W.; Vanderwall, D. E.; Turner, C. J.; Kozarich, J. W.; Stubbe, J. *J. Am. Chem. Soc.* **1996**, *118*, 1281.
(30) Caceres-Cortes, J.; Sugiyama, H.; Ikudome, K.; Saito, I.; Wang, A. H.-J. *Biochemistry* **1997**, *36*, 9995.
(31) Caceres-Cortes, J.; Sugiyama, H.; Ikudome, K.; Saito, I.; Wang, A. H.-J. *Eur. J. Biochem.* **1997**, *244*, 818.
(32) Wu, W.; Vanderwall, D. E.; Teramoto, S.; Lui, S. M.; Hoehn, S.; Tang, X.-J.; Turner, C. J.; Boger, D. L.; Kozarich, J. W.; Stubbe, J. *J. Am. Chem. Soc.* **1998**, *120*, 2239.
(33) Hoehn, S. T.; Junker, H.-D.; Bunt, R. C.; Turner, C. J.; Stubbe, J. *Biochemistry* **2001**, *40*, 5892.
(34) Zhao, C.; Xia, C.; Mao, Q.; Forsterling, H.; DeRose, E.; Antholine, W. E.; Subczynski, W. K.; Petering, D. H. *J. Inorg. Biochem.* **2002**, *91*, 259.
(35) Burger, R. M.; Horwitz, S. B.; Peisach, J. *Biochemistry* **1985**, *24*, 3623.
(36) Petersen, M.; Nielsen, C. B.; Nielsen, K. E.; Jensen, G. A.; Bondensgaard, K.; Singh, S. J.; Rajwanshi, V. K.; Koshkin, A. A.; Dahl, B. M.; Wengel, J.; Jacobsen, J. P. *J. Mol. Recognit.* **2000**, *13*, 44.
(37) Burger, R. M.; Peisach, J.; Blumberg, W. E.; Horwitz, S. B. *J. Biol. Chem.* **1979**, *254*, 10906.
(38) Veselov, A.; Sun, H.; Sienkiewicz, A.; Taylor, H.; Burger, R. M.; Scholes, C. P. *J. Am. Chem. Soc.* **1995**, *117*, 7508.
(39) Veselov, A.; Burger, R. M.; Scholes, C. P. *J. Am. Chem. Soc.* **1998**, *120*, 1030.
(40) Lukoyanov, D.; Burger, R. M.; Scholes, C. P. *J. Am. Chem. Soc.* **2001**, *123*, 12742.
(41) Sienkiewicz, A.; Smith, B. G.; Veselov, A.; Scholes, C. P. *Rev. Sci. Instrum.* **1996**, *67*, 2134.
(42) Veselov, A.; Sun, H.; Sienkiewicz, A.; Taylor, H.; Burger, R. M.; Scholes, C. P. *J. Am. Chem. Soc.* **1995**, *117*, 7508.
(43) Veselov, A. V.; Osborne, J. P.; Gennis, R. B.; Scholes, C. P. *J. Am. Chem. Soc.* **2000**, *122*, 8712.
(44) Zhao, Y.; Lukoyanov, D. A.; Toropov, Y. V.; Wu, K.; Shapleigh, J. P.; Scholes, C. P. *Biochemistry* **2002**, *41*, 7464.
(45) Murov, S. L. *Handbook of Photochemistry*, Decker: New York, 1973.
(46) Burger, R. M.; Horwitz, S. B.; Peisach, J.; Wittenberg, J. B. *J. Biol. Chem.* **1979**, *254*, 12299.
(47) Burger, R. M.; Peisach, J.; Horwitz, S. B. *J. Biol. Chem.* **1982**, *257*, 8612.
(48) Giloni, L.; Takeshita, M.; Johnson, F.; Iden, C.; Grollman, A. P. *J. Biol. Chem.* **1981**, *256*, 8608.
(49) Waravdekar, V. S.; Saslaw, L. D. *J. Biol. Chem.* **1959**, *234*, 1945.
(50) Povirk, L. F.; Wübker, W.; Köhnlein, W.; Hutchinson, F. *Nucleic Acids Res.* 1977, *4*, 3573.
(51) Hoffman, B. M.; DeRose, V. J.; Doan, P. E.; Gurbiel, R. J.; Houseman, A. L. P.; Telser, J. Metalloenzyme Active-Site Structure and Function through Multifrequency CW and Pulsed ENDOR. In *EMR of Magnetic Molecules*; Berliner, L. J., Reuben, J., Eds.; Plenum Press: New York, 1993; Vol. 13.
(52) Werst, M. M.; Davoust, C. E.; Hoffman, B. M. *J. Am. Chem. Soc.* **1991**, *113*, 1533.
(53) Burger, R. M.; Berkowitz, A. R.; Peisach, J.; Horwitz, S. B. *J. Biol. Chem.* **1980**, *255*, 11832.

(54) Sam, J. W.; Takahashi, S.; Lippai, I.; Peisach, J.; Rousseau, D. L. *J. Biol. Chem.* **1998**, *273*, 16090.

(55) Fann, Y.-C.; Gerber, N. C.; Osmulski, P. A.; Hager, L. P.; Sligar, S. G.; Hoffman, B. M. *J. Am. Chem. Soc.* **1994**, *116*, 5989.

(56) Fulmer, P.; Zhao, C.; Li, W.; DeRose, E.; Antholine, W. E.; Petering, D. H. *Biochemistry* **1997**, *36*, 4367.

(57) D'Andrea, A. D.; Haseltine, W. A. *Proc. Natl. Acad. Sci. U.S.A.* **1978**, *75*, 3608.

(58) Takeshita, M.; Grollman, A. P.; Ohtsubo, E.; Ohtsubo, H. *Proc. Natl. Acad. Sci. U.S.A.* **1978**, *75*, 5983.

(59) Rutter, R.; Hager, L. P. *J. Biol. Chem.* **1982**, *257*, 7958.